Fundamental Research xxx (xxxx) xxx

Contents lists available at ScienceDirect

Fundamental Research

journal homepage: http://www.keaipublishing.com/en/journals/fundamental-research/

Article

Uranium isotopes of aeolian dust deposited in northern Tibetan Plateau glaciers: Implications for tracing aeolian dust provenance

Xiaoyu Jiao[a,b], Zhiwen Dong[a,*], Janice Brahney[c], Eric J.R. Parteli[d], Fangzhou Li[e], Augusto Marcelli[f], Ting Wei[a]

[a] State Key Laboratory of Cryosphere Sciences, Northwest Institute of Eco-Environment and Resources, Chinese Academy of Sciences (CAS), Lanzhou 730000, China
[b] University of Chinese Academy of Sciences, Beijing 100049, China
[c] Department of Watershed Sciences, Utah State University, Logan, UT 84322, USA
[d] Faculty of Physics, University of Duisburg-Essen, Duisburg 47057, Germany
[e] School of Atmospheric Sciences, Sun Yat-sen University, Guangzhou 510275, China
[f] CNR - Istituto Struttura della Materia and Elettra-Sincrotrone Trieste, Basovizza Area Science Park, Trieste 34149, Italy

ARTICLE INFO

Article history:
Received 5 July 2021
Received in revised form 30 December 2021
Accepted 6 January 2022
Available online xxx

Keywords:
Uranium isotopes
Tibetan Plateau glaciers
Dust provenance tracing
Long range transport

ABSTRACT

Asian dust comprises a large portion of the northern hemisphere atmospheric dust load, thereby exerting substantial influence on the Earth's climate, global biogeochemistry and hydrological cycle through accelerated snow and ice melt. Dust deposited on alpine glaciers encodes information on broad scale atmospheric-environmental processes. The ($^{234}U/^{238}U$) values of dust fine particulates can reflect the comminuting time and intermediate processes; thus, it provides a new method for the provenance of aeolian dust in the glacial snowpack/cryoconite. Here we present results from a comprehensive survey of uranium isotopic concentrations in dust collected from cryoconites on the glaciers of the northern Tibetan Plateau (TP). These results indicate significant spatial heterogeneity in the ($^{234}U/^{238}U$) values associated with snowpack/cryoconite dust over a broad range of glaciers in the northern TP. The values of the ($^{234}U/^{238}U$) ratio in the glaciers of western Qilian Mountains (Qiyi Glacier, Shiyi Glacier, Laohugou Glacier No.12) were the highest, followed by the Tanggula (Dunkemadi Glacier) and Kunlun Mountains (Yuzhufeng Glacier), whereas these values were the lowest in the eastern Qilian Mountains (Jingyangling Snowpack, Dabanshan Snowpack, Lenglongling Glacier). By including the analysis of Sr-Nd isotopic compositions, we find the spatial isotopic distribution reflects a combination of local dust, which is associated with short comminuting times, and dust transported over long ranges. Meteorological data indicate that the dust production in the west and north TP, Alxa arid lands and Gobi Deserts, may have a significant impact on the TP glaciers. Moreover, U-Sr-Nd isotopic composition and end-member mixing models (EMMA) were used in our study to find out the relative contribution of distinct Asian dust sources to the dust budget in the TP glaciers. The results reveal that snowpack/cryoconite dust is derived from both local sources (low comminution signatures) as well as other dust sources in the Asian region. Our study demonstrates the potential of U isotope composition as a dust tracing method. In particular, by investigating this composition on dust collected from glacier snowpack and cryoconite holes, we arrive at a map of the distribution characteristics of ($^{234}U/^{238}U$) values in different regions of the TP. Our study is the first to deploy uranium comminution age for Tibetan dust source tracing, and the results are important to elucidate the multiple origins and dynamics of dust in the Tibetan Plateau.

1. Introduction

Aeolian mineral dust exerts a broad range of climatic and environmental impacts. For example, dust affects air quality and human health by transmitting, removing and depositing atmospheric pollutants [1,2], acts as cloud condensation nuclei, thereby affecting the climate, and provides a potential source of provide iron, phosphorus and micronutrient elements to remote marine and terrestrial ecosystems, thus influencing the carbon cycle [3,4]. Furthermore, aeolian dust is one of the key factors for the accelerated melting of glaciers. Various studies have shown that dust can significantly reduce the albedo of the glacier surface, thereby accelerating the melting of snow and ice [5,6]. Therefore, aeolian mineral dust may exert a substantial impact on the cryosphere.

Arid and semi-arid regions in northwest China are important dust sources in Asia and constitute key regions in studies of global climate change and regional environmental response [7]. Dust aerosols and chemical signatures in snow and ice samples from the Tibetan Plateau (TP) region of Asia can provide information on source regions and trans-

* Corresponding author.
E-mail address: dongzhiwen@lzb.ac.cn (Z. Dong).

https://doi.org/10.1016/j.fmre.2022.01.026

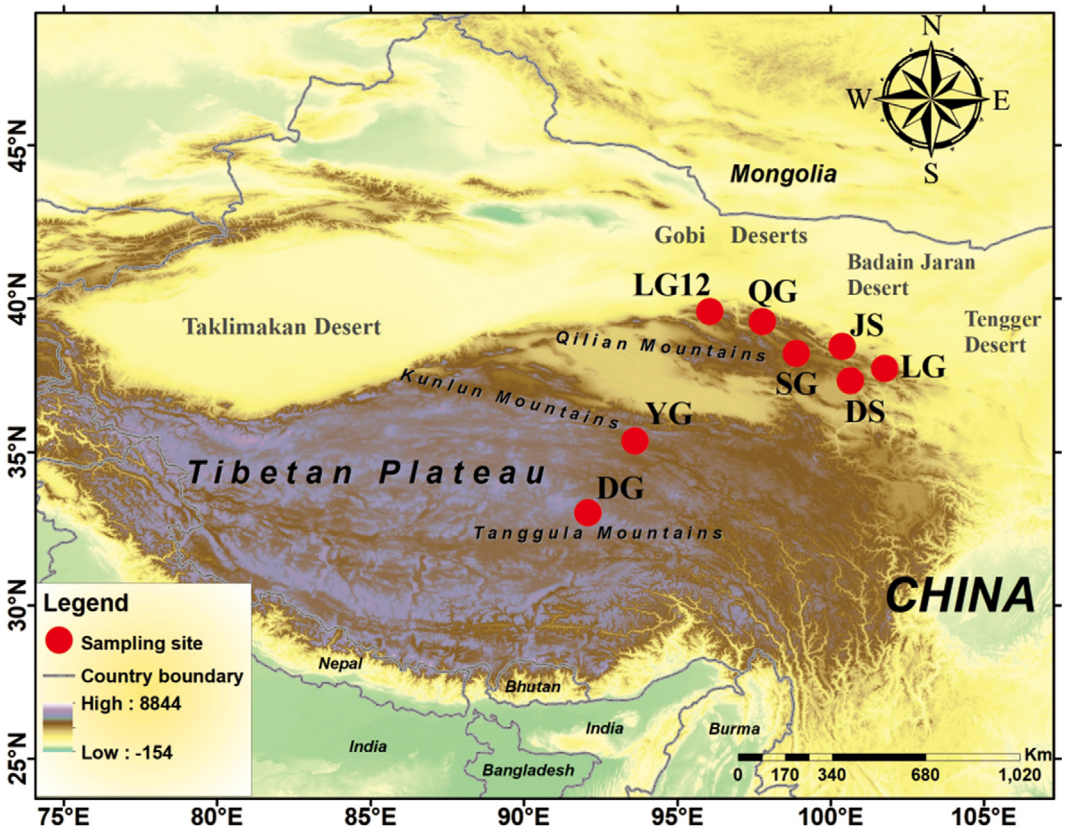

Fig. 1. Location map of study areas and sampling sites of the Tibetan Plateau (based on the standard map of China GS(2021)5448), including the Lenglongling Glacier (LG), Qiyi Glacier (QG), Shiyi Glacier (SG), Jingyangling Snowpack (JS), Laohugou Glacier No.12 (LG 12), Dabanshan Snowpack (DS) in the Qilian Mountains, and Dunkemadi Glacier (DG) in the Tanggula Mountains, and Yuzhufeng Glacier (YG) in the Kunlun Mountains.

port distances. In particular, dust deposited in high-altitude glaciers is associated with long transport distances and encodes information on a particulate matter within the upper troposphere and above the boundary layer [8,9]. Asian dust is transported far and wide by the high-altitude westerly jets and mid-to-low-altitude atmospheric circulation [10,11]. Direct observations and accurate extrapolation of meteorological satellite data [12] and backward air mass trajectory models [13] also indicate that the long-range transported Asian dust mainly originates from the large deserts of the Earth, including China's Western deserts and the Gobi Desert [14].

Different studies have indicated that the uranium isotope ($^{234}U/^{238}U$) ratio of fine particles (smaller than 50 μm) reflects the time elapsed since they were comminuted. Fine particles from different sources often have distinct fragmentation mechanisms, transport routes, and, thus, comminution times [15–17]. Therefore, different $^{234}U/^{238}U$ values may reflect multiple time and length-scales associated with atmospheric dust production, transportation and deposition.

Uranium comminution age has been successfully applied as a proxy for the origin of deep-sea sediments [15], river sediments [18–21], lake sediments [22], glacial basins [16] and loess sediments on the Chinese Loess Plateau [5,17]. Aeolian dust is mainly transported through suspension over high altitudes. During the transport process from the source to the high-altitude glacier, the comminution time of dust particles is insignificant and the $^{234}U/^{238}U$ will reflect the source [5,23]. Therefore, uranium isotopes can provide a new proxy for the provenance of aeolian dust in the snowpack/cryoconite of high-altitude glaciers on the TP.

TP is the youngest and most complex plateau in the world, giving birth to the largest glacial area of Earth's middle and low latitudes. TP plays an important role in the Asian monsoon circulation and also for the global climate system [24,25] . The aeolian dust deposited in the snow/ice of alpine glaciers on the TP and its surrounding areas has been topic of intense research [4,10,26–33]. However, none of these previous studies reported the observation of U isotopes.

In the present study, we use the mineral U isotope composition from dust collected from glacier snowpack and cryoconite holes to map the spatial distribution of ($^{234}U/^{238}U$) values in different regions of the TP. To the best of our knowledge, our study is the first to deploy the uranium comminution age for dust source tracing. We combine the U dust source tracking with existing Sr-Nd isotope and meteorological data to constrain the sources, transport routes, and transport distance of Asian aeolian dust. Our study shows that U constitutes a powerful isotope tracer for glacier dust provenance.

2. Data and methods

Snowpack/cryoconite dust samples (Figs. 1 and 2) were collected from several glaciers of the northern TP (both from the northeast and central areas), including the Lenglongling Glacier (LG), Jingyangling Snowpack (JS), Dabanshan Snowpack (DS) in the eastern Qilian Mountains of the northeast TP, Qiyi Glacier (QG), Shiyi Glacier (SG), Laohugou Glacier No.12 (LG12) in the west Qilian Mountains, Yuzhufeng Glacier (YG) in the Kunlun Mountains, and Dunkemadi Glacier (DG) in the Tanggula Mountains of central TP. The snowpack/cryoconite dust samples were collected during the spring and summer of 2017–2019, and a total of 27 snowpack/cryoconite samples were collected for detection and composition analysis of U isotopes. The detailed information about the studied glaciers is provided in Table 1.

Fig. 2. Images showing the glacier snowpack and cryoconite sampling on glaciers of the northern Tibetan Plateau, including the Yuzhufeng Glacier (YG, (a)), Laohugou Glacier No.12 (LG 12, (b)), and Dabanshan Snowpack (DS, (c)) and Qiyi Glacier (QG, (d)).

Table 1
Information on sampling location, elevation at various mountain glaciers of the northern Tibetan Plateau.

Sites	Mountains	Latitude(N)	Longitude(E)	Altitude(m a.s.l.)	Sample type
Dabanshan Snowpack (DS)	Qilian Mountains	37°21′	101°24′	3593–3625	Snowpack/cryoconite
Shiyi Glacier (SG)	Qilian Mountains	38°12′	99°52′	4035–4303	Snowpack/cryoconite
Laohugou Glacier No.12 (LG12)	Qilian Mountains	39°29′	96°31′	4450–4850	Snowpack/cryoconite
Qiyi Glacier (QG)	Qilian Mountains	39°08′	97°27′	4500–4680	Snowpack/cryoconite
Jingyangling Snowpack (JS)	Qilian Mountains	37°50′	101°06′	3700–3990	Glacier surface snow/cryoconite
Lenglongling Glacier (LG)	Qilian Mountains	37°30′	101°32′	3557–3780	Glacier surface snow/cryoconite
Yuzhufeng Glacier (YG)	Kunlun Mountains	35°39′	94°14′	4480–4720	Snowpack/cryoconite
Dunkemadi Glacier (DG)	Tanggula Mountains	33°04′	92°04′	5464–5714	Snowpack/cryoconite

2.1. Sample pretreatment and measurements

The collected snowpack/cryoconite samples were dried, then the dust was first immersed in 0.5 mol/L diluted acetic acid for 2 h at room temperature to disperse and remove the carbonate minerals. Thereafter, the samples were processed using an electroforming sieve to separate particle sizes 10–50 μm. In our measurements, owing to the instrument limitations, only particle sizes smaller than < 50 μm can be analyzed with regard to the ratio change of $^{234}U/^{238}U$ [15,21]. At the same time, previous research indicated that the uncertainty of particle comminution time caused by particle size can be effectively reduced as long as the particle size is controlled within a certain range [21]. In the present study, samples with a particle size range of 10–50 μm were selected for uranium comminution age analysis. Within such particle size range, the U isotope comminution age fits within the ideal range [15,16]. The overall trend of ($^{234}U/^{238}U$) value decreases with the age of the granular material.

After sieving, the samples were reduced and leached to remove Fe-Mn oxides, hydroxides, and other non-detritus materials in a dithionite-citrate solution buffered with sodium bicarbonate. Then, the samples were soaked in hydrogen peroxide to remove organic matter. HF-HNO_3 was then used to digest the silicate minerals and we used UTEVA ion exchange resin to separate U. U isotopic ratios were measured by means of a Plasma II multi-receiving inductively coupled plasma mass spectrometer (MC-ICP-MS), in which ^{238}U is collected in a Faraday cup, while ^{234}U is collected in a secondary electron multiplier. We used the SSB (Standard Sample Bracketing) method to correct the short-term variation of the instrument [17]. The 2σ standard deviation of the ($^{234}U/^{238}U$) ratio indicated by the MC-ICP-MS was 0.001. Instrumental bias between ^{234}U and ^{238}U was corrected by normalizing the $^{238}U/^{235}U$ ratio to 137.84. The long-term measurement result of the international standard USGS BCR-2 reference material ($^{234}U/^{238}U$) is 1.001 ± 0.003 (n = 20, 2σ), which is consistent with the internationally recognized ratio within the error range.

2.2. Uranium comminution age method

The principle is based on the recoiling effect during alpha (α) decay of ^{238}U. The ^{234}U in the rock is the product of ^{238}U undergoing one α decay to ^{234}Th and then undergoing two β decays. The unstable ^{234}U will continue to undergo α decay to become ^{230}Th. Therefore, after several U series decays (about 1 Ma), the U isotope in the bedrock will reach an equilibrium state, that is, the production rate of ^{234}U (owing to the

decay of ^{238}U) is equal to the decay rate of ^{234}U (into ^{230}Th):

$$\lambda_{238} \cdot {}^{238}U = \lambda_{234} \cdot {}^{234}U \quad (1)$$

In Eq. (1), λ_{234} denotes the decay constant of ^{234}U and amounts to, approximately, 2.82206×10^{-6}/a. Furthermore, $\lambda_{238} \approx 1.55125 \times 10^{-10}$/a is the decay constant of ^{238}U [5]. Since the absolute ratio of ^{234}U/^{238}U is very small, it is usually expressed as the radioactivity ratio (^{234}U/^{238}U):

$$(^{234}U/^{238}U) = \frac{\lambda_{234} \cdot {}^{234}U}{\lambda_{238} \cdot {}^{238}U}$$

Under initial equilibrium conditions, the value of (^{234}U/^{238}U) is equal to 1. Therefore, a secular equilibrium would be disturbed once fine particles (≤50 μm) are generated because a significant portion of ^{234}U is ejected out of the particle due to the recoil effect during α-decay of ^{238}U, thereby rendering the ^{234}U particle accumulation rate smaller than the decay rate [15,21]. The (^{234}U/^{238}U) will thus gradually decrease in time from the onset of comminuting, until the new steady-state equilibrium is reached. Correspondingly, the value of (^{234}U/^{238}U) can record the time elapsed from dust generation to the fine particles' measurement, thus making it possible to track intermediate processes from comminution to deposition.

2.3. FY-4A meteorological satellite observation and CALIPSO/CALIOP data analysis

To shed further light on the potential source areas and transport routes of aeolian dust, we used the true-color dust detection image of FY-4A meteorological observation satellite of China National Meteorological Satellite Center (http://www.nsmc.org.cn/) to analyze dust storm progressions over the TP and its surrounding areas during the sampling period. CALIPSO (Cloud-Aerosol Lidar and Infrared Path finder Satellite Observations) /CALIOP (Cloud-Aerosol Lidar with Orthogonal Polarization) data [30] (http://www-calipso.larc.nasa.gov/) were used to analyze the vertical distribution of aerosols and determine the aerosol type of the TP and its surrounding areas. NOAA (National Oceanic and Atmospheric Administration), NCAR (National Center for Atmospheric Reanalysis) /NCEP (National Centers for Environmental Prediction) wind field data (derived from https://www.esrl.noaa.gov/) were used to represent regional and large-scale atmospheric circulation information. Using the aforementioned meteorological satellite data, the source and possible transport path of dust in the northern TP were evaluated.

2.4. End-member mixing analysis (EMMA)

We determined the relative contribution of dust sources to the mixed dust samples collected from the glaciers using End-Member Mixing Analysis (EMMA). The method was initially developed for stream source separation techniques and later adapted for use in sediment and dust unmixing [5,34–36]. The conditions required are that (1) the end-member sources are identifiable and conservative, and (2) the mixed samples are bound by all potential end-members. The method can also be used to certify that all likely sources have been identified [36]. The percent contribution from each end-member is computed in εNd-(^{234}U/^{238}U) mixing space using least-squares regression equations. Potentially contributing dust sources included the Gobi Deserts, Alxa Arid Lands, and TP surface dust.

3. Results and discussion

3.1. Uranium isotopic composition of snowpack/cryoconite dust from several glaciers of the northern TP

Fig. 3 shows the uranium isotope (^{234}U/^{238}U) distribution in snowpack/cryoconite dust from several glaciers of the northern TP (including the northeast and central). The highest (^{234}U/^{238}U) value (0.999) occurred for the cryoconite dust sample No. 2 of YG, as well as for the snow dust sample 30-1 of LG 12. This value indicates that the dust in the cryoconite/snowpack has a short comminution time. Moreover, the lowest value was 0.950 and was measured for the cryoconite dust sample No. 1 of YG. The average (^{234}U/^{238}U) values of SG, LG12 and QG of the western Qilian Mountains are generally high, amounting to 0.972, 0.978 and 0.984, respectively. To compare, the average (^{234}U/^{238}U) value for DG in the central TP is 0.975, while (^{234}U/^{238}U) values in JS, LG and DS of the east Qilian Mountains are generally low. In particular, the lowest average value is 0.957 in DS, while the average value of YG in the Kunlun Mountains is 0.97. In general, the (^{234}U/^{238}U) values of glaciers showed a general decreasing trend from the west Qilian-Tanggula Mountains to the Kunlun Mountains and to the east Qilian Mountains.

Table 2 displays the geographic spatial distribution information of the sample's sites and of the U isotopic composition. The (^{234}U/^{238}U) values in snowpack/cryoconite dust samples of QG, LG 12, and YG exhibited two major distributional ranges. One is the high value range that is close to the equilibrium value, and the other is a low value range (0.950 to 0.961 for YG, 0.973 to 0.976 for QG, and 0.965 to 0.979 for LG 12). The (^{234}U/^{238}U) values in JS (0.980, 0.962) and DG (0.979, 0.966) were also significantly different. The distribution of (^{234}U/^{238}U) values in LG (ranging from 0.965 to 0.969) and DS (ranging from 0.956 to 0.958) was relatively narrow. Sr isotope differences in northern TP are not significant (except for YG, where the ^{87}Sr/^{86}Sr is 0.7148 to 0.7218), the corresponding (^{234}U/^{238}U) values are mainly distributed between 0.7188 and 0.7231. However, the distinction of Nd isotopes is obvious. DG of Tanggula Mountain has the lowest εNd value, between -14.7 and -13.9. The εNd values of YG in the Kunlun Mountains mainly range from -13.4 to -10.6, and the Qilian Mountains (SG, JS and LG) host the highest values (ranging from -10.9 to -8.9).

Fig. 4 shows the spatial distribution of U-Nd-Sr isotopic composition of snowpack/cryoconite dust, as well as of some local surface dust from various glaciers. As can be seen from the U-Nd in Fig. 4a, the U-Nd isotopic composition in snowpack/cryoconite dust of different glaciers is significantly different. LG and SG in the Qilian Mountains have the highest εNd values (ranging from -10.9 to -9.1), and the (^{234}U/^{238}U) value is low (ranging from 0.964 to 0.976). Furthermore, DS in the Qilian Mountains has a relatively low εNd value (ranging from -12.1 to -12.0), as well as a low value of (^{234}U/^{238}U) ranging from 0.956 to 0.958. However, the εNd value of DG in Tanggula Mountain is the lowest (ranging from -14.7 to -13.9), while the (^{234}U/^{238}U) value is relatively high, and ranges from 0.966 to 0.979. The highest ^{87}Sr/^{86}Sr value was detected in the DG (0.7251), while the lowest ^{87}Sr/^{86}Sr value was found in the YG (0.7148). The ^{87}Sr/^{86}Sr values of Qilian Mountains were mainly distributed within the range from 0.7191 to 0.7231 (Fig. 4b). Moreover, the U-Nd-Sr isotopic composition of different snowpack/cryoconite dust samples from the same glacier (Fig. 4a and b) also varied greatly (e.g., QG, YG and LG12).

The U-Sr-Nd isotopic composition of glacier snowpack/cryoconite dust with higher (^{234}U/^{238}U) values in QG, LG12 and YG is very similar to that of local surface dust (Fig. 4). We infer that the local surface soil dust, which has a relatively short comminution time, may originate from erosion of the glaciers. Strong glaciation [2,21,37] may explain the emergence of a significant concentration of dust fragments s with balanced values of (^{234}U/^{238}U), which can be attributed to a short comminution time. We found that, in LG12 and DS, the Sr-Nd isotopic composition of snowpack/cryoconite dust is very similar to that of the local surface soil dust, while the (^{234}U/^{238}U) value is comparatively lower (Fig. 4). This local surface soil dust is interpreted here as granular material with a long comminution time. Once fine particulates are produced, they are stored *in situ*. After a long period of deposition, the (^{234}U/^{238}U) value of surface soil dust gradually decreases over time, and under the influence of the current geological and atmospheric circulation conditions, the dust is transported to high-altitude glaciers.

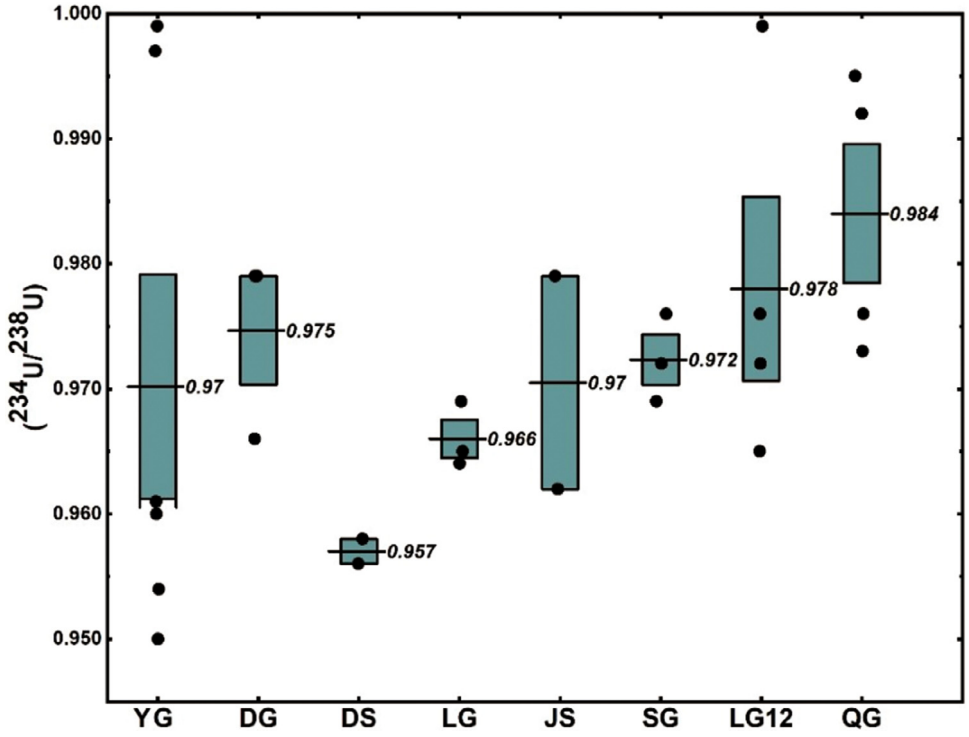

Fig. 3. The figure showing the distribution of ($^{234}U/^{238}U$) values of all glaciers in the study area, including Lenglongling Glacier (LG), Qiyi Glacier (QG), Shiyi Glacier (SG), Jingyangling Snowpack (JS), Laohugou Glacier No.12 (LG 12), Dabanshan Snowpack (DS), and Dunkemadi Glacier (DG), and Yuzhufeng Glacier (YG). The blue boxes indicate the range of standard deviation, the long straight lines are the mean values, and the black dots are the ($^{234}U/^{238}U$) values of the sampling points.

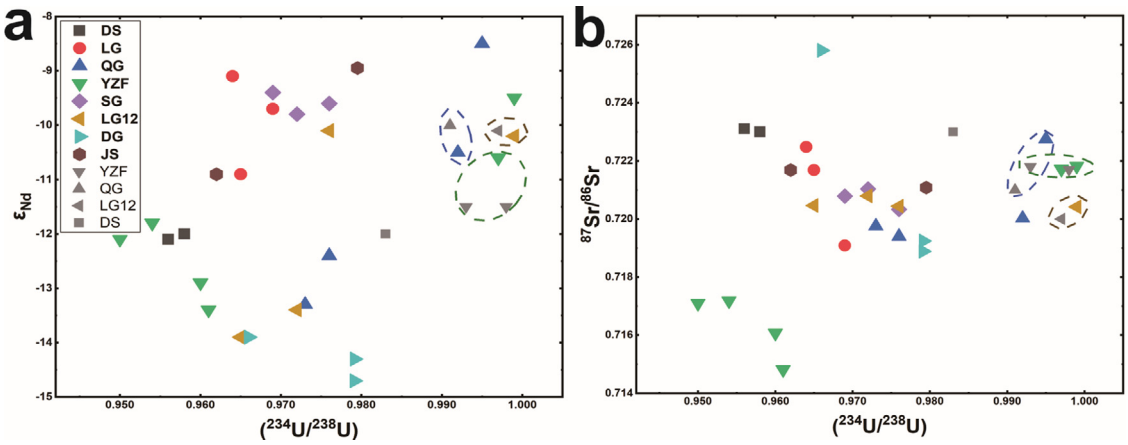

Fig. 4. U-Sr-Nd isotopic composition of cryoconite/snowpack in various regions of the Tibetan Plateau, and comparison with local soil. The gray signs in the figure are the corresponded local soil data, including the Yuzhufeng Glacier (YG), Qiyi Glacier (QG), Dabanshan Snowpack (DS) and Laohugou Glacier No.12 (LG 12) [4,7,47].

In general, the ($^{234}U/^{238}U$) values of snowpack/cryoconite dust in various remote regions display clear differences in the spatial distribution. These differences in the spatial distribution of ($^{234}U/^{238}U$) values may indicate differences in the dust sources and transport routes. Moreover, the occurrence of different ($^{234}U/^{238}U$) values within the same glacier dust system attest to the multiple origins of the local aeolian dust.

We note that the particle size effect can be generally neglected when this particle size is generally smaller than 50 μm. Owing to the limited resolution associated with our measurements, the ratio changes of $^{234}U/^{238}U$ are detected only when the particle size is small enough (usually < 50 μm) [15,21,38]. Previous research indicated that the uncertainty of particle comminution time caused by particle size can be effectively reduced as long as the particle size is controlled within a certain range [21]. Our previous particle size tests on glacier snowpack/cryoconite dust on the Tibetan Plateau showed that the particle size of dust deposited in high-altitude glacier snowpack/cryoconite falls within the range from 0.57 to 20 μm (long range transported dust). Moreover, the associated mode of particle size distribution is about 10 to 15 μm. This particle size distribution lies below the range from 20 to 100 μm associated with the local dust (particle number ratio smaller than 20%), which has mode about 40 μm [7,8,10,31].

We have also measured the particle size distribution of surface dust samples on the TP, thereby finding that the particle size is generally

Table 2
U isotopic compositions in glacier snowpack/cryoconite of various study locations of the Tibetan Plateau.

Samples	Locations	Latitude(°N)	Longitude(°E)	Altitude(m a.s.l.)	Sample type	($^{234}U/^{238}U$)	2*SD
DS snow 5	Dabanshan Snowpack	37.35	101.40	3593.0	snow	0.958	0.0018
DS snow 3	Dabanshan Snowpack	37.35	101.40	3625.0	snow	0.956	0.0015
LG cryoconite 6	Lenglongling Glacier	37.51	101.54	3780.0	cryoconite	0.969	0.0007
LG cryoconite 11	Lenglongling Glacier	37.51	101.54	3557.5	cryoconite	0.964	0.0008
LG cryoconite 9	Lenglongling Glacier	37.51	101.54	3732.0	cryoconite	0.965	0.0017
QG cryoconite 1	Qiyi Glacier	39.14	97.45	4680.0	cryoconite	0.992	0.0012
QG cryoconite 5	Qiyi Glacier	39.14	97.45	4500.0	cryoconite	0.973	0.0011
QG cryoconite 6	Qiyi Glacier	39.14	97.45	4580.0	cryoconite	0.976	0.0004
QG cryoconite 8	Qiyi Glacier	39.14	97.45	4480.0	cryoconite	0.995	0.0009
YG snow/cryoconite 1	Yuzhufeng Glacier	35.65	94.23	4531.0	snow/cryoconite	0.950	0.0019
YG snow/cryoconite 3	Yuzhufeng Glacier	35.65	94.23	4558.0	snow/cryoconite	0.954	0.0008
YG snow/cryoconite 5	Yuzhufeng Glacier	35.65	94.23	4540.0	snow/cryoconite	0.961	0.0027
YG snow/cryoconite 8	Yuzhufeng Glacier	35.65	94.23	4480.0	snow/cryoconite	0.960	0.0027
YG snow/cryoconite 7	Yuzhufeng Glacier	35.65	94.23	4720.0	snow/cryoconite	0.997	0.0014
YG snow/cryoconite 2	Yuzhufeng Glacier	35.65	94.23	4620.0	snow/cryoconite	0.999	0.0005
SG cryoconite 1	Shiyi Glacier	38.20	99.86	4303.0	cryoconite	0.976	0.0012
SG cryoconite 2	Shiyi Glacier	38.20	99.86	4152.0	cryoconite	0.972	0.0007
SG cryoconite 3	Shiyi Glacier	38.20	99.86	4035.0	cryoconite	0.969	0.0007
LG12 snow 30-1	Laohugou Glacier No.12	39.48	96.52	4849.0	snow	0.999	0.0012
LG12 snow 8	Laohugou Glacier No.12	39.48	96.52	4850.0	snow	0.972	0.0001
LG12 cryoconite 16	Laohugou Glacier No.12	39.48	96.52	4590.0	cryoconite	0.976	0.0011
LG12 cryoconite 29-4	Laohugou Glacier No.12	39.48	96.52	4450.0	cryoconite	0.965	0.0001
DG cryoconite 18-18	Dunkemadi Glacier	33.07	92.07	5604.0	cryoconite	0.966	0.0001
DG cryoconite 19-10	Dunkemadi Glacier	33.07	92.07	5464.0	cryoconite	0.979	0.0020
DG cryoconite 19-19	Dunkemadi Glacier	33.07	92.07	5714.0	cryoconite	0.979	0.0001
JS snow 14	Jingyangling Snowpack	37.83	101.10	3700.0	snow	0.980	0.0009
JS snow 15	Jingyangling Snowpack	37.83	101.10	3990.0	snow	0.962	0.0013

smaller than 100 μm (Fig. S1) [29]. Therefore, in this study, samples with a particle size range of 10–50 μm were selected for uranium comminution age analysis. Within such particle size range, the U isotope comminution age falls within the ideal range [15,16], and the data reflect the overall trend of ($^{234}U/^{238}U$) value decreasing with the increase of age. Therefore, we find that the particle size composition of the TP glacial dust is very similar in each region [4,31]. The variations in U isotope upon changes in particle size should fall within the measurement error bars and will not cause much scatter of the U isotope data in the results.

3.2. Source and transport routes of dust over northern TP based on meteorological satellite data

Geosynchronous meteorological satellites with large imaging ranges and high observation frequency yields a powerful means for monitoring the temporal and spatial variation of dust. FY-4A constitutes a new generation of geostationary meteorological satellites in China [39]. It is loaded with a variety of observation instruments and can provide 32 kinds of quantitative products. including cloud detection, marine and land aerosol detection, and sand detection products. The higher temporal and spatial resolution makes it possible to track the temporal and spatial distribution of dust, the dynamics of sandstorms and the atmospheric dust path.

Based on the FY-4A meteorological satellite true-color dust storm detection map from China National Satellite Meteorological Center (Fig. 5) (http://www.nsmc.org.cn/), it has been possible to track the diffusion path and intensity change of the dust during a sandstorm on April 3, 2020. At 04:00 UTC on April 3 (Fig. 5a), dust appeared first in the west TP and Gobi Desert, occurring thereafter in Xinjiang's Taklimakan Desert and Alxa Plateau arid areas (Fig. 5b). The dust gradually spread to the surroundings, and the dust intensity increased slightly with time (Fig. 5c and d). Owing to the characteristics of the atmospheric circulation (Fig. 6), the dust could be transported further and further to a larger area. Therefore, dust from west TP, south Gobi Desert [8] and Alxa arid region are likely to have an impact on the glaciers of TP. The dust from the TP itself (surface soil dust and arid lands) provides an important source of the glaciers dust due to the expanding arid deserts of the TP [40]. Moreover, it is reasonable to conclude that the Taklimakan Desert yields a potential source for the long-range transported dust in the glaciers of northern TP, considering the Westerly winds and frequent dust storm emissions from the Taklimakan Desert. Dust from the Taklimakan Desert is known to travel long distances and remain aloft for prolonged time periods [41–43].

CALIPSO is a cloud-aerosol Lidar and infrared explorer observation satellite jointly developed by National Aeronautics and Space Administration (NASA) and the French National Space Research Center (CNES). The CALIOP satellite-borne Lidar instrument can obtain the vertical distribution characteristics of dust. This instrument is able to detect the vertical distribution of aerosols [44] and can distinguish aerosol types, thus yielding useful data support for dust prediction and related scientific research [45]. Fig. 6 shows the diurnal variation of wind field during the dust storm process on April 3, 2020 (Fig. 6a and b) and the attenuated backscatter coefficient (km-1sr-1) profile at 532 nm, with 60 m vertical and 12 km (Fig. 6c) horizontal resolution over the TP and its surrounding areas (http://www-calipso.larc.nasa.gov). Fig. 7 shows the distribution of four-season wind fields on the TP and East Asia. The main aerosol components in this large range are dust, polluted smog, and dust (Fig. 6c). As illustrated in Figs. 6a, b, and 7, the pollutants from south Gobi Desert and Alxa arid region could be delivered to the north TP.

Fengyun meteorological satellite images and wind field data provide information on the temporal and spatial changes of potential dust sources and transport routes, and CALIOP/CALIPSO data provide more detailed information on the spatial distribution, physical and optical properties of aerosol pollutants, etc. This provides us with meteorological data support for further distinguishing the sources and transport routes of each glacier dust.

3.3. Dust sources based on U isotope fingerprinting

Fig. 8 displays the distribution of U-Sr-Nd isotopic composition of snowpack /cryoconite dust in the study area, as well as of the surface soil dust in the potential dust source areas based on the available data. In this figure, different colored areas indicate the isotopic composition range of potential dust source areas in Asia, including different regions

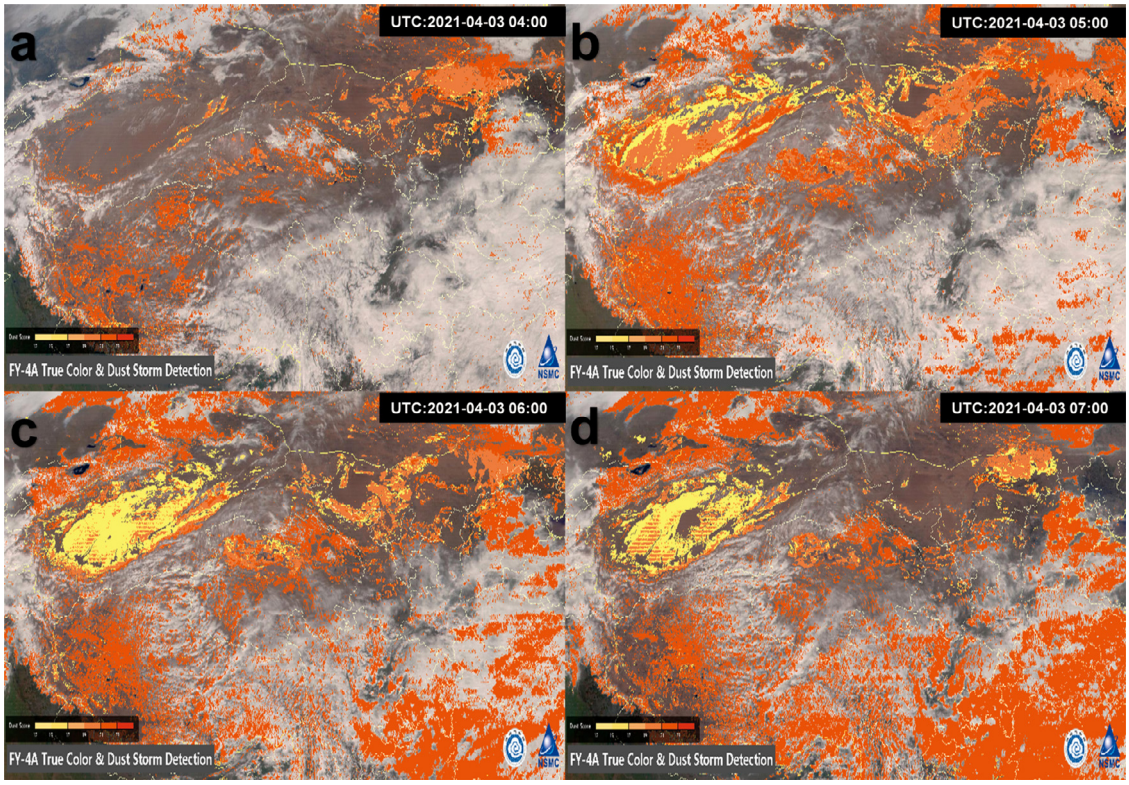

Fig. 5. FY-4A meteorological satellite true color dust storm detection image, showing the transport process of dust emission from Tibetan Plateau. Yellow-orange-red indicates the dust detected and the intensity of the dust. The image is derived from China's National Satellite Meteorological Center.

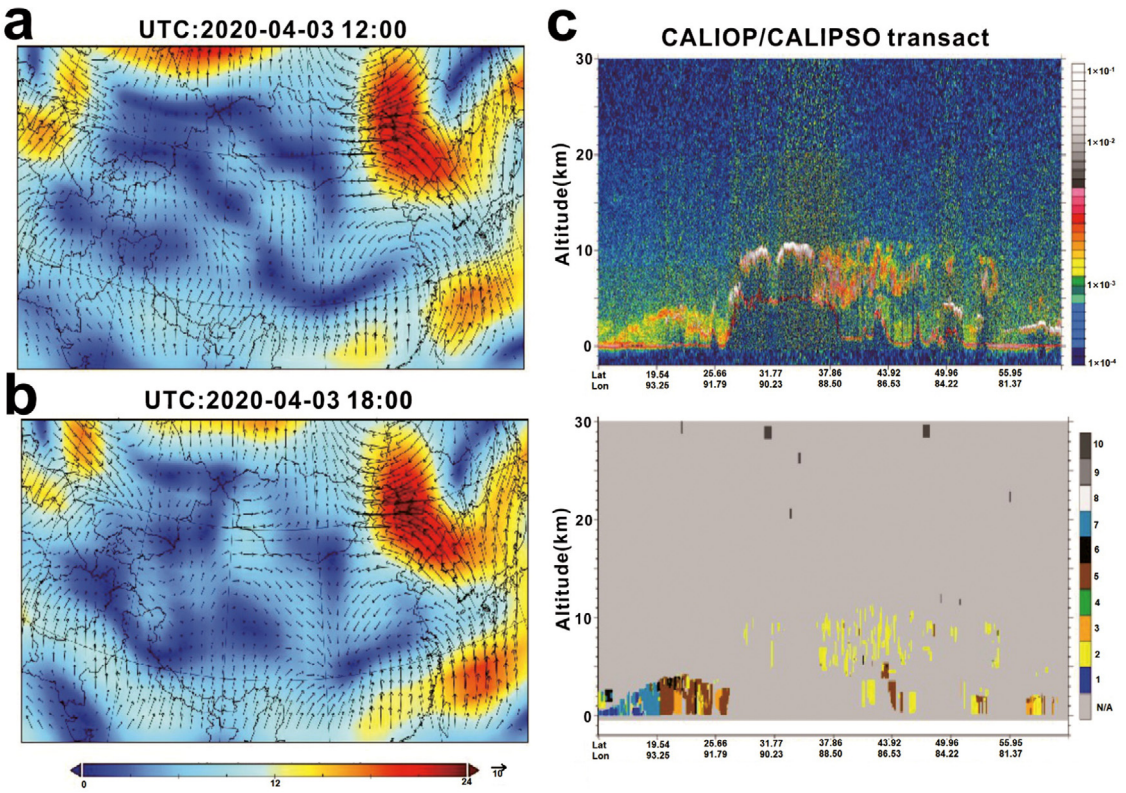

Fig. 6. Spatial distribution of wind vectors (m s^{-1}) at 700 hPa over the Tibetan Plateau and its surrounding areas from 12 to 18 UTC, April 3 and CALIOP/CALIPSO transact showing attenuated backscatter coefficient (km^{-1} sr^{-1}) profiles at 532 nm with 60 m vertical and 12 km horizontal resolution and aerosol type over the Tibetan Plateau (TP) and its surrounding area. The outline of the topography is shown as a solid orange line. Thick clouds appear in white and pollutants and dust clouds in orange-red.

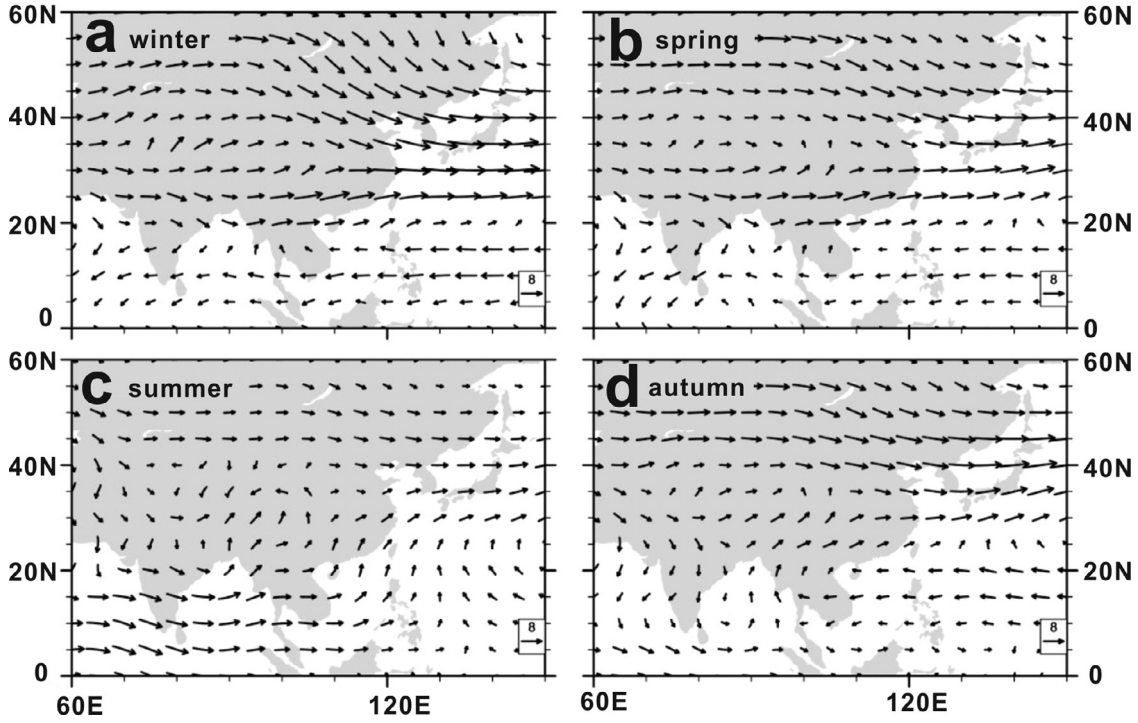

Fig. 7. Mean wind field in study area during each season of 2016–2020, reflecting the potential dust transport routes in Tibetan Plateau and surroudings, based on National Centers for Environmental Prediction/National Center for Atmospheric reanalysis data.

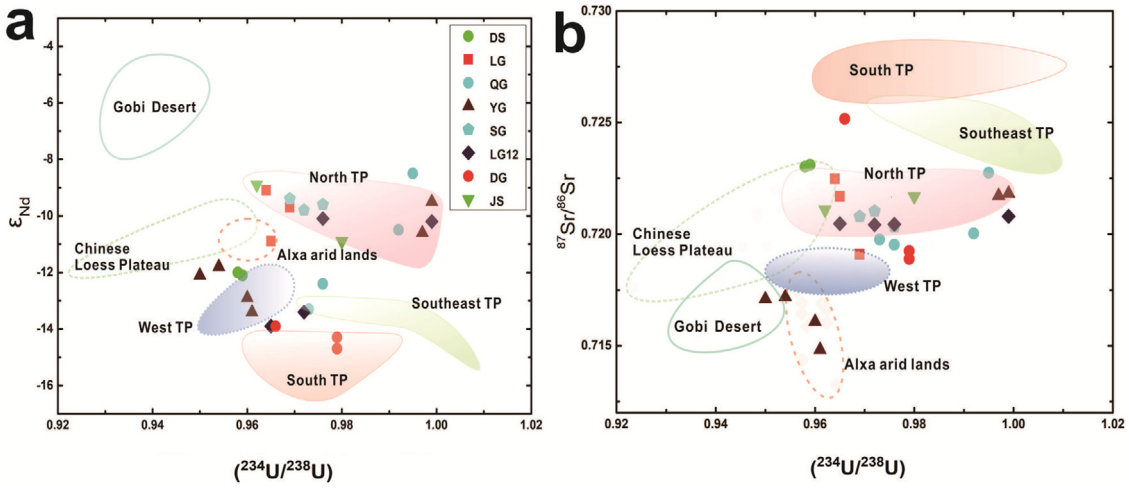

Fig. 8. Comparison of the U-Sr-Nd isotopic composition of the cryoconite/snowpack dust in the Tibetan Plateau with other major dust sources in the Northern Hemisphere, including Gobi Desert (south), Alxa arid lands, Chinese Loess Plateau and the surface soil dust of Tibetan Plateau [4,5,7,46,47].

of TP (west, north, south and southeast), Gobi Desert (south) and Alxa arid lands (including Badain Jaran Desert, Tengger Desert and their surrounding areas), and Chinese Loess Plateau [5,46]. The U-Sr-Nd isotopic composition of surface soil dust in different potential source areas has different geographical distribution characteristics (Fig. 8). Moreover, the isotopic composition of surface soil dust in Gobi Desert is clearly different and associated with high εNd value, low $^{87}Sr/^{86}Sr$ value and low ($^{234}U/^{238}U$) value. The U-Sr isotopic composition of the surface soil dust over the TP is comparatively higher, while the εNd value is generally lower (but slightly higher in the north TP). The $^{87}Sr/^{86}Sr$ value of Alxa arid lands is low, and the U-Nd is within an intermediate range between the values in TP and Gobi Desert.

Furthermore, clear heterogeneity in the spatial distribution was found in the U-Sr-Nd isotopic composition of snowpack/cryoconite dust from various glaciers. In general, the isotopic composition characteristics of dust deposited in the Qilian Mountains, such as LG 12, QG, SG, YG and LG are similar to the isotopic composition characteristics of the dust in the north and west TP [47], and in the Alxa arid region. The results from these isotope measurements indicate relatively similar long-distance dust sources and transport routes over the glaciers of north TP. However, the snowpack/cryoconite dust isotopic composition of the DG in the central TP resemble those of surface soil dust in west and south TP, and clearly differ from the corresponding composition of Gobi Desert surface soil dust. The distinct isotopic composition of dust deposited over different glaciers attests for different atmospheric transport routes and dust sources between the Qilian and Tanggula Mountains.

Based on meteorological data, the dust source and transport routes in the study area were identified, and the potential source areas in different glaciers were further distinguished by combining uranium comminution

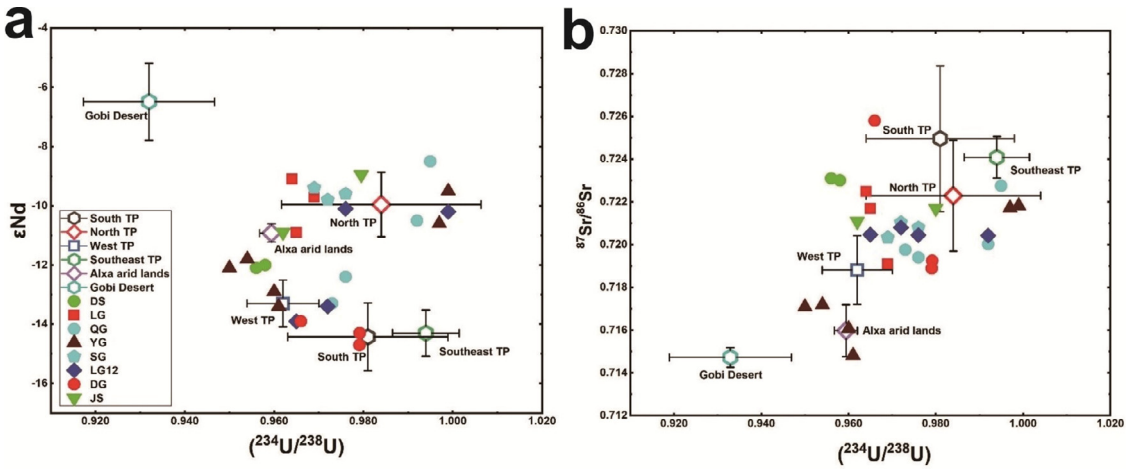

Fig. 9. The U-Sr-Nd isotopic composition of the cryoconite and snowpack dust in the Glaciers of the Tibetan Plateau and the potential dust sources in the Asian, including Gobi Desert (south), Alxa arid lands and the surface dust from different regions of the Tibetan Plateau [4,5,7,46,47]. The center point is the mean value, with error bars showing standard error of the mean.

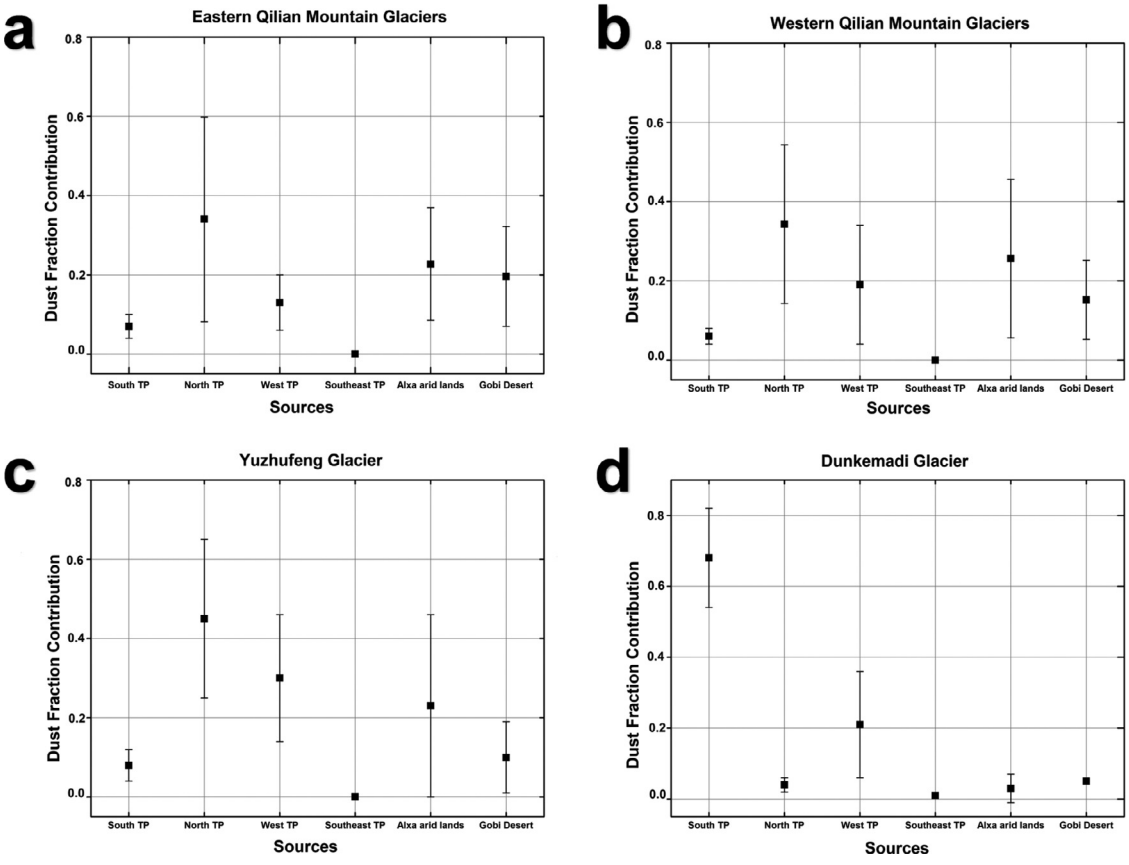

Fig. 10. Dust sources and sinks obtained based on isotope mixing space model. The mean and distribution of each source was used to determine the mean relative contribution to each sink. Potentially contributing dust sources included the Gobi Deserts, Alxa Arid Lands, and TP surface dust.

age and Sr-Nd isotopic geochemistry. We believe that the glaciers in the north TP are mainly affected by dust imports from the north TP (including dust near the local glaciers), the west TP [4,10] and the Alxa arid region. DG in the central TP is mainly affected by the west and south TP.

To further elucidate the contribution of Asian dust transport to the glacier dust budget in the study area, we used the End-Member Mixing models (EMMA) to calculate the ratios of dust sources to the sinks in TP (Fig. 9). The contribution percentage of each end-member to dust sinks is computed in εNd-($^{234}U/^{238}U$) mixing space using least-squares regression equations. Available data on potential contributing dust sources included the Gobi Desert, Alxa Arid lands, and TP surface soil dust. These data showed that in eastern Qilian Mountains, dusts from north TP contributed about 16–65% of the dusts in the glaciers and snowpacks (JS, LG and DS), with an average contribution of 34%, and the west TP contributed 5–20%, with an average contribution of 13%. To compare, and the Alxa arid lands contributed about 7–27%, with an average contribution of 13%, while the contribution of Gobi Desert is about 12–30%,

with an average contribution of 19%. For the glaciers in the western Qilian Mountains (SG, QG and LG 12), the dust contribution of the north TP is about 25–70%, with an average contribution of 34%, and the west TP is 8–25%, with an average contribution of 19%. Furthermore, Alxa arid lands contributes about 15–35% of the dust with an average contribution of 25%. For the YG in Kunlun Mountains, the north TP contributed the most, namely, about 50% of the dusts in the glacier, while the Alxa arid lands and the Gobi Deserts contributed 24% and 10%, respectively.

The glacier dust of the DG of Tanggula Mountain is mainly from the south and west TP, accounting for about 68% and 20%, respectively (Fig. 10). These results further indicate that the high-altitude glaciers in the TP are mainly affected by dust transport and deposition on the surface of the TP itself, as well as dust income from the Great Deserts of North China [47]. Moreover, previous studies further show that the Taklimakan Desert also contributes to the input of glacier dust to the northern TP [4,47].

Therefore, in the present study, we demonstrate the use of U isotope composition as a novel tracer method, based on analysis of dust collected of glacier snowpack and cryoconite holes to map the distribution characteristics of ($^{234}U/^{238}U$) values in different regions of the TP. In particular, to the best of our knowledge, our study is the first to deploy uranium comminution age for dust source tracing in the Tibetan Plateau.

4. Conclusions

Aeolian dust from snowpack/cryoconite repositories encodes information about current and past atmospheric and environmental processes. In the Tibetan Plateau (TP), the high-altitude glaciers provide a record of dust paths above the boundary layer in the upper troposphere, thereby reflecting regional to long-range aeolian transport characteristics.

The uranium comminution age method can be used to trace the intermediate processes in the dust cycle from production and transport to deposition associated with the different comminuting times. Aeolian dust can be transported from the source areas to the high-altitude glaciers within days or hours. Based on the large spatial scale of our sample area and uranium isotopic analyses of snowpack/cryoconites dust on the glaciers of the northern TP, we found that the ($^{234}U/^{238}U$) of snowpack/cryoconite dust in different regions showed significant spatial differences. The general ($^{234}U/^{238}U$) ratio in the glacial dust of western Qilian Mountains (QG, SG, LG12) showed a higher value, followed by the Tanggula (DG) and Kunlun Mountains (YG), whereas in the eastern Qilian Mountains (JS, DS, LG) ($^{234}U/^{238}U$) ratio displayed the lowest value. Based on these results, and considering the associated Sr-Nd isotopic compositions, the observed spatial distribution can be attributed to a combination of local dust, which has a short comminuting time, and dust transported over a long range.

Using FY-4A dust monitoring, as well as NOAA, NCAR/NCEP meteorological and CALIPSO/ CALIPOP data, the analysis of the present work shows that the dust from the west and south TP, south Gobi Desert and Alxa arid region constitutes a major source of the dust deposited in the TP. U-Sr-Nd isotopic composition data and analysis with EMMA revealed that incoming dust in the glaciers of the east Qilian Mountains in the north TP, such as LG, DS and JS, is provenance mainly from the north TP and Alxa arid Deserts, the dust contribution amounting to 16–65% and 7–27%, respectively. The LG 12, QG and SG in the west Qilian Mountains are mainly affected by the north and west TP, which contribute 25–70% and 8–25% of the incoming dust, respectively. The north TP contributes the most to the dust input from YG of Kunlun Mountains, accounting for about 50% of the dust. DG of the Tanggula Mountain in the central TP is mainly derived from the dust in the south and west TP, accounting for about 68% and 20% of the dust budget, respectively.

Therefore, the present study demonstrated the potential of U isotope as a novel tracer to track dust age. In combination, with other isotopic tracers, U isotope can provide a powerful method for the identification of dust sources and transport paths. Our study is the first to use uranium comminution age for Tibetan dust source tracing, and the insights gained from our results can be used in future studies to elucidate the multiple origins of dust in the TP glaciers, as well as the dynamics of regional-scale dust circulation and deposition throughout the Tibetan Plateau.

Declaration of Competing Interest

The authors declare that they have no conflicts of interest in this work.

Acknowledgments

This work was funded by the National Natural Science Foundation of China (42022002), and the State Key Laboratory of Cryosphere Sciences (SKLCS-ZZ-2021). JB is funded through NSF Critical Zone Collaborative proposal #2011910, while EJRP thanks the German Research Foundation (DFG) for funding through the Heisenberg Programme “Multiscale Simulation of Earth Surface Processes”. The authors would like to thank the NOAA, NCEP/NCAR for sharing the regional and global wind field data, and the true-color dust detection image of FY-4A meteorological observation satellite of China National Meteorological Satellite Center. And also, many thanks to the fieldwork team (Li G, Chen S) who worked in the harsh and cold environment on the Tibetan Plateau.

Supplementary materials

Supplementary material associated with this article can be found, in the online version, at doi:10.1016/j.fmre.2022.01.026.

References

[1] K.E. Wilkening, L.A. Barrie, M. Engle, Trans-pacific air pollution, Science 290 (5489) (2000) 65–67.
[2] Y.K. Li, D.W. Li, G.N. Liu, et al., Patterns of landscape evolution on the central and northern Tibetan Plateau investigated using *in-situ* produced 10Be concentrations from river sediments, Earth Planet. Sci. Lett. 398 (2014) 77–89.
[3] T.D. Jickells, Z.S. An, K.K. Andersen, et al., Global iron connections between desert dust, ocean biogeochemical, and climate, Science 308 (5718) (2005) 67–71.
[4] Z.W. Dong, Y.P. Shao, D.H. Qin, et al., Hf-Nd-Sr isotopic composition as fingerprint for long-range transported eolian dust deposition in glacier snowpack of eastern Tibetan Plateau, J. Geophys. Res. Atmos. 123 (2018) 7013–7023.
[5] L. Li, J. Chen, Y. Chen, et al., Uranium isotopic constraints on the provenance of dust on the Chinese Loess Plateau, Geology 46 (9) (2018) 747–750.
[6] Y.L. Zhang, S.C. Kang, Z.Y. Cong, et al., Light absorbing impurities enhance glacier albedo reduction in the southeastern Tibetan Plateau, J. Geophys. Res. Atmos. 122 (2017) 6915–6933.
[7] Z.W. Dong, S.C. Kang, D.H. Qin, et al., Provenance of cryoconite deposited on the glaciers of the Tibetan Plateau: new insights from Nd-Sr isotopic composition and size distribution, J. Geophys. Res. Atmos. 121 (12) (2016) 7371–7382.
[8] Z.W. Dong, D.H. Qin, S.C. Kang, et al., Physicochemical characteristics and sources of atmospheric dust deposition in snow packs on the glaciers of western Qilian Mountains, China, Tellus B 66 (2014) 20956.
[9] G.X. Wu, C.L. Zhang, X.L. Zhang, et al., The environmental implications for dust in high-alpine snow and ice cores in Asian mountains, Glob. Planet. Chang. 124 (2015) 22–29.
[10] Z.W. Dong, D.H. Qin, J.Z. Chen, et al., Physicochemical impacts of dust particles on alpine glacier meltwater at the Laohugou Glacier basin in western Qilian Mountains, China, Sci. Total Environ. 493 (2014) 930–942.
[11] Y.P. Shao, C.H. Dong, A review on East Asian dust storm climate, modelling and monitoring, Global Planet. Chang. 52 (1-4) (2006) 1–22.
[12] J.M. Prospero, P. Ginoux, O. Torres, et al., Environmental characterization of global sources of atmospheric soli dust identified with the NIMBUS 7 total ozone mapping spectrometer (TOMS) absorbing aerosol product, Rev. Geophys. 40 (2002) 1002.
[13] R.R. Draxler, G.D. Rolph, HYSPLIT (Hybrid Single-Particle Lagrangian Integrated Trajectory) Model Access via NOAA ARL READY, NOAA Air Resources Laboratory, Silver Spring, MD, 2003.
[14] Z.B. Dong, G.Y. Hu, G.Q. Qian, et al., High-altitude aeolian research on the Tibetan Plateau, Rev. Geophys. 55 (4) (2017) 864–901.
[15] D.J. DePaolo, K. Maher, J.N. Christensen, et al., Sediment transport time measured with U-series isotopes: results from ODP North Atlantic drift site 984, Earth Planet. Sci. Lett. 248 (2006) 394–410.
[16] D.J. DePaolo, V.E. Lee, J.N. Christensen, et al., Uranium comminution ages: sediment transport and deposition time scales, C.R. Geosci. 344 (2012) 678–687.
[17] L. Li, X.J. Liu, T. Li, et al., Uranium comminution age tested by the eolian deposits on the Chinese Loess Plateau, Earth Planet. Sci. Lett. 467 (2017) 64–71.

[18] A. Dosseto, S.P. Turner, G.B. Douglas, Uranium-series isotopes in colloids and suspended sediments: timescale for sediment production and transport in the Murray—Darling River system, Earth Planet. Sci. Lett. 246 (2006) 418–431.
[19] F. Chabaux, E. Blaes, M. Granet, et al., Determination of transfer time for sediments in alluvial plains using ^{238}U-^{234}U-^{230}Th disequilibria: the case of the Ganges River system, C.R. Geosci. 344 (2012) 688–703.
[20] H.K. Handley, S. Turner, J.C. Afonso, et al., Sediment residence times constrained by uranium-series isotopes: a critical appraisal of the comminution approach, Geochim. Cosmochim. Acta 103 (2013) 245–262.
[21] V.E. Lee, D.J. DePaolo, J.N. Christensen, Uranium-series comminution ages of continental sediments: case study of a Pleistocene alluvial fan, Earth Planet. Sci. Lett. 296 (2010) 244–254.
[22] A. Francke, A. Dosseto, J. Just, et al., Assessment of the controls on (^{234}U/^{238}U) activity ratios recorded in detrital lacustrine sediments, Chem. Geol. 550 (2020) 119698.
[23] Y.H. Fu, L. Li, J. Chen, Application of uranium isotope chronology for practical comminution in the eolian dust system, Adv. Earth Sci. 33 (10) (2018) 1031–1047 (In Chinese).
[24] G.X. Wu, Y.M. Liu, B. He, et al., Thermal controls on the Asian summer monsoon, Sci. Rep. 2 (2012) 4.
[25] M.X. Yang, X.J. Wang, G.J. Pang, et al., The Tibetan Plateau cryosphere: observations and model simulations for current status and recent changes, Earth Sci. Rev. 190 (2019) 353–369.
[26] G.J. Li, J. Chen, J.F. Ji, Natural and anthropogenic sources of East Asian dust, Geology 37 (2009) 727–730.
[27] J.Z. Xu, G.M. Yu, S.C. Kang, et al., Sr-Nd isotope evidence for modern aeolian dust sources in mountain glaciers of Western China, J. Glaciol. 58 (211) (2012) 859–865.
[28] T.D. Yao, L.G. Thompson, V. Mosbrugger, et al., Third Pole Environment (TPE), Environ. Dev. 3 (1) (2012) 52–64.
[29] T. Wei, J. Brahney, Z.W. Dong, et al., Hf-Nd-Sr isotopic composition of the Tibetan Plateau dust as a fingerprint for regional to hemispherical transport, Environ. Sci. Technol. 55 (2021) 10121–10132.
[30] Z.H. Du, C.D. Xiao, Y.Z. Wang, et al., Dust provenance in Pan-third pole modern glacierized regions: what is the regional source, Environ. Pollut. 250 (2019) 762–772.
[31] Z.W. Dong, J. Brahney, S.C. Kang, et al., Aeolian dust transport, cycle and influences in high-elevation cryosphere of the Tibetan Plateau region: new evidences from alpine snow and ice, Earth Sci. Rev. 211 (2020) 103408.
[32] Z.W. Dong, Z.Q. Li, F.T. Wang, et al., Characteristics of atmospheric dust deposition in snow on the glaciers of the eastern Tien Shan, China, J. Glaciol. 55 (193) (2009) 797–804.
[33] G.X. Wu, X.L. Zhang, C.L. Zhang, et al., Mineralogical and morphological properties of individual dust particles in ice cores from the Tibetan Plateau, J. Glaciol. 62 (231) (2016) 46–53.
[34] J. Brahney, A.P. Ballantyne, M. Vandergoes, et al., Increased dust deposition in New Zealand related to twentieth century Australian land use, J. Geophys. Res. 124 (2019) 1181–1193.
[35] J. Brahney, J.J. Clague, B. Menounos, et al., Geochemical reconstruction of late Holocene drainage and mixing in Kluane Lake, Yukon Territory, J. Paleolimnol. 40 (1) (2008) 489–505.
[36] N. Christophersen, C. Neal, R.P. Hooper, et al., Modeling stream water chemistry as a mixture of soil water end-members—a step towards 2nd generation acidification models, J. Hydrol. 116 (1–4) (1990) 307–320.
[37] F. Herman, D. Seward, P.G. Valla, et al., Worldwide acceleration of mountain erosion under a cooling climate, Nature 504 (2013) 423–426.
[38] B.A. Maher, J.M. Prospero, D. Mackie, et al., Global connections between aeolian dust, climate and ocean biogeochemistry at the present day and at the last glacial maximum, Earth Sci. Rev. 99 (1-2) (2010) 61–97.
[39] M. Min, C.Q. Wu, C. Li, et al., Developing the science product algorithm test bed for chinese next-generation geostationary meteorological satellites: fengyun-4 series, J. Meteorol. Res. 31 (4) (2017) 708–719 2017.
[40] R.P. Zu, Z.L. He, Y.M. Zong, et al., Review on the influences of sand accumulation on permafrost in the Tibetan Plateau, J. Desert Res. 34 (5) (2014) 1208–1214 (in Chinese).
[41] J.M. Sun, M.Y. Zhang, T.S. Liu, Spatial and temporal characteristics of dust storms in China and its surrounding regions, 1960–1999: relations to source area and climate, J. Geophys. Res. 106 (D10) (2001) 10325–10333.
[42] J. Xuan, I.N. Sokolik, J. Hao, et al., Identification and characterization of sources of atmospheric mineral dust in East Asia, Atmos. Environ. 38 (36) (2004) 6239–6252.
[43] N. Nagatsuka, N. Takeuchi, T. Nakano, et al., Geographical variations in Sr and Nd isotopic ratios of cryoconite on Asian glaciers, Environ. Res. Lett. 9 (2014) 045007.
[44] M.A. Vaughan, K.A. Powell, D.M. Winker, et al., Fully automated detection of cloud and aerosol layers in the CALIPSO lidar measurements, J. Atmos. Ocean. Technol. 26 (10) (2008) 2034–2050.
[45] N.B. Lakshmi, V.S. Nair, S.S. Babu, Vertical structure of aerosols and mineral dust over the bay of bengal from multi-satellite observations: mineral dust over the Bay of Bengal, J. Geophys. Res. Atmos. 122 (23) (2017) 12,845–12,861.
[46] J. Chen, G.J. Li, J.D. Yang, et al., Nd and Sr isotopic characteristics of Chinese deserts: implications for the provenances of Asian dust, Geochim. Cosmochim. Acta 71 (2007) 3904–3914.
[47] T. Wei, Z.W. Dong, S.C. Kang, et al., Hf-Nd-Sr isotopic fingerprinting for aeolian dust deposited on glaciers in the northeastern Tibetan Plateau region, Glob. Planet. Chang. 177 (2019) 69–80.

Xiaoyu Jiao, a graduate student at the State Key Laboratory of Cryosphere Sciences, Northwest Institute of Eco-Environment and Resources, Chinese Academy of Sciences. The main research work is focused on the emission, transport and land surface process of aeolian dust using the uranium isotopes in the glacier areas of the Tibetan Plateau and surrounding regions.

Zhiwen Dong, Ph.D., Professor at the State Key Laboratory of Cryosphere Sciences, Northwest Institute of Eco-Environment and Resources, Chinese Academy of Sciences. Funded by the National Science Foundation for Excellent Young Scholars in 2020, and his work mainly engaged in the transport and diffusion of aeolian dust and pollutants and their climate effects in cryospheric regions. He applied the new methods of high-resolution transmission electron microscopy (TEM-EDX) for single particle observation in aerosols of the cryosphere regions and improved the isotopic geochemical evidence to conduct systematic studies of aeolian dust and pollutants transport process and influence in western China and Tibetan Plateau.